Optimisation Algorithms for Multi-Group Energy Structures

M. J. Fleming[a,b,*], L. W. G. Morgan[a], E. Shwageraus[b]

[a] *CCFE, Culham Science Centre, Abingdon, Oxon, OX14 3DB, United Kingdom*
[b] *Department of Engineering, University of Cambridge, Trumpington Street, Cambridge CB2 1PZ, United Kingdom*

Abstract

Modelling of nuclide densities as a function of time within magnetic confinement fusion devices such as the JET, ITER and proposed DEMO tokamaks is performed using Monte-Carlo transport codes coupled with a Bateman equation solver. The generation of reaction rates occurs either through point-wise interpolation of energy dependent tracked particle data with nuclear data or multi-group convolution of 'binned' fluxes with binned cross-sections. The multi-group approach benefits from decreased computational expense and data portability, but introduces errors through effects such as self-shielding. Depending on the multi-group structure and nuclear data used, this method can introduce unacceptable errors without warning. We present a multi-group optimisation method which utilises a modified particle swarm algorithm to generate seed solutions for a non-stochastic 'string-tightening' algorithm. This procedure has been used with a semi-homogenised 1D DEMO-like reactor design in order to produce an optimised energy group structure for tritium breeding. In this example, the errors introduced by the Vitamin-J 175 multi-group are reduced by two orders-of-magnitude in the optimised group structure.

Keywords: Fusion neutronics, Monte-Carlo, Multi-group, MCNP, Reaction rate, ITER, DEMO

1. Introduction

One of the great benefits of Monte-Carlo (MC) particle transport codes such as MCNP [1] lies in the fact that phase space does not need to be specifically discretised. MC codes take advantage of the full, continuous energy data – although at the cost of execution time and local nature of practically obtainable outputs, such as flux tallies. MC transport codes track individual particles and sample nuclear data files to simulate reactions. They can be used to interpolate point-wise (PW) between data points for reaction rate calculation or fluxes can be recorded in some discrete energy multi-group (MG) and later collapsed with nuclear data. While PW calculations enjoy greater accuracy, MG methods are still of fundamental importance due to computational resource limits and data

*Corresponding author
Email address: michael.fleming@ccfe.ac.uk (M. J. Fleming)

portability. MC calculations using PW convolutions (for example, the `FM` multipliers of MCNP) must refer to and interpolate within nuclear data for each reaction – in addition to running the transport calculations. When using energy bin multipliers (as provided by another code or the `EM` multipliers of MCNP), the user specifies the cross-section for a set of bins and MCNP will simply tally the population in each bin before taking the convolution of histograms. This benefits from a significant decrease in the computational expense when compared with PW convolution – particularly when a large set of reaction rates are required. While a 'point-wise flux' is effectively calculated through the set of all particles which are tallied, this data cannot be used by other software, such as inventory codes. MG fluxes and effective cross-sections can be easily used as inputs for other codes which can perform whatever user-specific tasks which are not within the capabilities of MCNP[1].

As a simplified integral method MG convolution can only provide approximate values of reaction rates, but it also suffers from systematic errors due to numerous factors such as self-shielding, which is temperature and material composition specific. A recent study found that several thousand groups would be necessary to meet desired accuracy for fusion applications, when bins were chosen as equal lethargy [2], although fewer would be required with self-shielding corrections. For this study non-resonant reactions are considered to demonstrate the optimisation method without the complexities of MG resonance treatment.

We present an optimisation for MG energy group structure which we use to limit MG deviations from PW calculation. It has been demonstrated that the Vitamin-J 175 group structure[2] overestimates total tritium-producing effective cross-sections [5]. To demonstrate the capabilities of this optimisation, it has been employed to decrease the MG error in the tritium-yielding reactions which occur in the blanket modules of a simplified DEMO-like reactor. The optimisation performed in this study can easily be applied to other reactor designs or sets of reactions relevant to other systems.

2. Optimisation Methods

The goal of this study is to minimise the PW-MG collapsed cross section difference by determining an optimal MG energy discretisation. Each discretisation with n groups represents one vector in an $(n-1)$-dimensional space. For every possible multi-group in this space, there is a total PW-MG collapsed cross section difference[3]:

$$\sigma(PW) - \sigma(MG) \equiv \frac{1}{\phi}\left[\left(\int_{E_{min}}^{E_{max}} \sigma(E)\phi(E)dE\right) - \sum_{i=1}^{n} \sigma_i\phi_i\right]. \quad (1)$$

While minimising this difference is the ultimate goal, using it as the fitness function for minimisation would result in some MG where compensating over- and under-estimations returned no error. Instead, the sum of the square deviations in each group j, for each tested MG i,

[1] Such as multi-phase irradiation pulses which cannot be accurately handled by CINDER - a common issue for fusion analysis.

[2] Whose raison d'être is fusion neutronics and shielding [3, 4].

[3] This is still a minor idealisation, since PW convolution is not truly continuous.

$$f_{i,j} \equiv f(x_{i,j}) = \left[\left(\int_{x_{j-1}}^{x_j} \sigma(x)\phi(x)dx \right) - \sigma_j \phi_j \right]^2 , \quad (2)$$

is used for optimisation of the MG. While a non-stochastic algorithm will be employed to find the optimal MG, it requires an informed seed MG which must be found from a large parameter space. To probe this multi-dimensional space with a fitness function which takes the time required for an MCNP simulation (with individual bin variance much less than PW-MG deviation) and has numerous deep minima, we employ a stochastic algorithm which uses 'swarm intelligence' [6]. This concept requires multiple test solutions (multi-groups) to be tracked simultaneously. The fitness $f_i = \sum_j f_{i,j}$ for each MG indexed by i is also recorded and new test solutions are generated in each iteration based on a combination of random walks from the previous test solutions coupled with directed movement toward the best MGs already found. Collective knowledge can be implicitly created through the sharing of information between the multiple test solutions, which are referred to as a 'swarm'. As one of a variety of swarm-based optimisations that have seen wide use, particle swarm optimisation (PSO) [7] benefits from being (and was chosen in this study because it has) a simple core concept that is easy to implement and easily modified in a surprising number of ways for adaptation to problem-specific features.

During each iteration, the algorithm generates group-wise evaluated nuclear data files (GENDFs) for each reaction and for each MG. These are used to automatically generate MCNP inputs which will be executed to calculate MG and PW reaction rates over each bin for each MG. The square of the PW-MG deviation from equation (2) is determined for each bin and is summed to provide a fitness value for each test solution. Each of the $(n-1)$-dimensional positions are updated by swarm-guided motion before the new multi-groups are used in the next iteration.

The units in all deviations-per-bin figures are (barns/source neutron)^2. The MG fitness, $f_i = \sum_j f_{i,j}$, is used by the PSO algorithm to update energy group structures using a random walk coupled with pulls toward personal, local and/or global best positions. To do this, a global best MG is recorded as a vector g_j and for each i a 'personal' best vector $p_{i,j}$ is kept. We follow the standard PSO implementation where in each iteration the positions are moved by addition of a vector $v_{i,j}$ based upon the best personal MG for each individual and the global best energy group as:

$$\begin{aligned} x_{i,j}[t+1] &= x_{i,j}[t] + v_{i,j}[t] & (3) \\ v_{i,j}[t+1] &= v_{i,j}[t]I[t] + c_1[t]r_1\left(p_{i,j} - x_{i,j}[t]\right) & (4) \\ &\quad + c_2[t]r_2\left(g_{i,j} - x_{i,j}[t]\right). \end{aligned}$$

In addition, iteration-dependent $I[t]$, personal preference $c_1[t]$ and global preference $c_2[t]$ parameters are varied over the course of the optimisation, along with the random numbers r_1, r_2 which are re-sampled for every call. In addition to this position motion, we add a modification which removes from each MG the bin with the best fitness $\{x_{i,b} | f_{i,b} < f_{i,j\neq b}\}$ and adds a position near the worst energy bin $\{x_{i,w} | f_{i,w} > f_{i,j\neq w}\}$. This can be controlled with a threshold parameter (*ie* only if $f_{i,b} < k f_{i,w}$, for some k) to speed up migration of energy groups over large energy ranges.

While PSO can probe a large subset of the parameter space, it cannot practically identify a specific pattern such as equal lethargy. The output of a PSO run should still

have large variance over bin fitness, as seen in Figure 1. The goal of a MG optimisation will be the minimisation of the differences in PW-MG deviations over all bins, into what we will refer to as the 'ideal' MG. While this energy structure and the constant PW-MG deviation is not known *a priori*, we include the average of the final output from section 4 in Figure 1. The PSO MG output is then used as the seed for a non-stochastic 'string tightening' algorithm. This algorithm still employs stochastic transport simulations, but we simulate enough particles to keep the transport statistical errors well below the magnitude of the PW-MG deviations. The position updates are given by the vectors[4]:

$$v_j = T\left(x_j - x_{j-1}\right)\left(\frac{f_{j+1} - f_j}{f_{j+1} + f_j}\right) \quad \text{if } f_j > f_{j+1} \tag{5}$$

$$v_j = T\left(x_{j+1} - x_j\right)\left(\frac{f_{j+1} - f_j}{f_{j+1} + f_j}\right) \quad \text{if } f_j < f_{j+1}. \tag{6}$$

The parameter T determines how far each bin can be pulled/pushed by a neighbour and must be less than 0.5 – if $T = 0.5$ and $f_{i+1}[t] \gg f_i[t]$, then we can obtain overlapping bins $f_{j-1}[t+1] = f_j[t+1]$. Bins with larger errors pull the nearby group boundaries toward their energy boundaries, leading to migration of bin density toward regions with greater overall error. As shown in Figure 2, the algorithm minimises local deviations in PW-MG error, followed by migration of energy bin density through error 'waves'.

As the PW-MG deviations decrease, the statistical variation of the transport calculation becomes relatively greater and the stochastic nature of the fitness function will generate fluctuations which prevent the optimisation from progressing. Additionally, threshold reactions will cause large fluctuations where bins jump between either containing the reaction or not.

3. Software

Nuclear data processing is performed by the NJOY processing system [8], a FORTRAN-90 code which calls modules sequentially to produce and modify data for specific applications. For our purposes the following modules are used:

- `RECONR` – Reconstructs the resonances and produces PENDF data
- `BROADR` – Adds temperature-dependent Doppler broadening of resonances
- `UNRESR` – Produces 'effective self-shielded' cross-sections, using average value resonance data from ENDF
- `THERMR` – Generates neutron scattering cross-sections for (temperature-specific) thermal energies
- `ACER` – Prepares ACE format libraries for use by MCNP

[4] *nb* Our convention was to take f_j to sum the group immediately below energy x_j, and there is only one energy group being tested in each iteration, so we omit the MG index i from before.

- `GROUPR` – Creates multi-group data with multiple subroutines designed to counter possible error introduction, including the Bondarenko narrow-resonance scheme [9] and user-specified weighting flux[5]

The optimisation procedure that was implemented utilised the point-wise convolution capabilities of MCNP which will call upon the ACE files. We therefore must use PENDF files processed in the same manner (and from the same raw source) to create ACE and GENDF data, as shown in Figure 3. All NJOY modules except `GROUPR` are called before the optimisation algorithm loop to produce PENDF and ACE files, while the optimisation will make repeated use of `GROUPR` to produce new GENDFs in each iteration.

The `F4` tallies of MCNP use `EM` energy multipliers with two sets of data: MG energy bin-cutoffs with arbitrary MG constants. We take the cross-sections from GENDF files to generate MG convolved reaction rates. The tally can also use `FM` tallies which interpolate within the PW ACE files. Comparing these for each bin, as in equation (2), generates our fitness function.

Throughout the optimisation the statical error in each bin should remain significantly less than the PW-MG deviation for the algorithm to continue improving the MG structure. This can become extremely demanding for a fine MG, where huge simulation time is required to obtain good individual bin statistics. We generally allow larger uncertainties in early iterations and increase the number of particles simulated (`nps`) to around 1E8 in the final iterations. For more realistic, non-spherical, heterogeneous models this would require considerably greater `nps`.

4. Tritium Breeding Blanket Test Case

We modelled a ceramic lithium orthosilicate pebble blanket with a low pressure helium purge gas[6]. This was layered with beryllium slabs which were separated by Eurofer sheets and high pressure helium coolant channels. The remaining structural materials were a mixture of Eurofer and Inconel-718 steels and magnets made of a niobium-tin superconductor, as will be used in ITER. These are the materials used in many DEMO studies and their nuclide fractions are summarised in Table A.2 of Appendix A.

The optimisation was performed on a spherical reactor with concentric shells of homogenised material. Each of the blanket layers contained the same mixture and radial variation of the flux was dealt with by splitting the 60cm blanket into four 15cm sections. A geometric cross-section of the reactor is presented in Figure 4 and the material composition of each of the cells is given, with the specific boundary radii, in Table 1.

The ^{6}Li, ^{7}Li and ^{9}Be are responsible for virtually all tritium production within proposed blanket modules for fusion reactors and their total (n,Xt) cross-sections are shown in Figure 5. Note that this set of reactions contains no narrow resonances and the total reaction rate for tritium production will be dominated by lower-energy ^{6}Li reactions.

[5] This methodology allows the calculation of multiple dilution-specific cross-sections to correct for self-shielding. Additionally, multiple-dilution group data can be processed by `MATXSR` for use with codes such as TRANSX [10]. We avoid these issues with our choice of reactions in this paper and use infinitely dilute data with the `iwt=8` 'fusion peak' weighting of NJOY.

[6] Based on one of the EU breeder module designs [11].

For our fitness function we have used the sum over all square PW-MG deviations of each tritium-producing reaction:

$$f_{i,j} = f_{i,j}(^6\mathrm{Li}) + f_{i,j}(^7\mathrm{Li}) + f_{i,j}(^9\mathrm{Be}). \tag{7}$$

For PSO the choice of seed solutions are, due to the stochastic nature of the optimisation and limited number of algorithm iterations possible, of tremendous importance. The balance we must reach rests between selecting seeds which are close enough to the ideal solution in order to limit execution time while being distant enough to probe a large subset of the space of multi-groups. The modified particle swarm algorithm was run with 20 seed MGs, each of which contain three groups of equal lethargy bins, so that N energies between E_1 and E_2 are given by

$$E_i = E_1 \exp\left\{\frac{i}{N}\log\left(\frac{E_2}{E_1}\right)\right\} \quad i = 0, \ldots, N. \tag{8}$$

N_T (themal) energies were chosen between 10^{-2} and 1 eV, N_I (intermediate) between 1 and 10^6 eV and N_F (fast) between 1 and 19.64 MeV, with a variety chosen for different seeds. The initial seed values for MG $j = 0, 1, \ldots, 19$ were taken as

$$N_{T_j} = 5 + j \; N_{I_j} = 115 - \left\lfloor \frac{j}{2} \right\rfloor \; N_{F_j} = 55 - \left\lceil \frac{j}{2} \right\rceil,$$

with floor and ceiling functions, respectively. After 145 iterations, the global best sum of squared deviations was reduced by nearly four orders of magnitude, from the Vitamin-J value of 4.84×10^{-15} to 7.31×10^{-19}. The PW-MG differences are in reactions per source neutron per cm^2. These tiny numbers are recorded for reproducibility, while the ratio provides an indication of the increase in MG performance. A second run was carried out with modified initial conditions. Seeds in the second optimisation were constructed in the same manner as the first, but the three-region bin numbers were based off of the results of the first run, where the global best energy group structure contained 38 energies below 1 eV, 125 between 1 eV and 1 MeV and 13 above 1 MeV. The second set of seeds were then taken as

$$N_{T_j} = 33 + \left\lceil \frac{j}{2} \right\rceil \; N_{I_j} = 127 - \left\lfloor \frac{j+1}{4} \right\rfloor \; N_{F_j} = 16 - \left\lfloor \frac{j+3}{4} \right\rfloor.$$

This second optimisation resulted in a global best energy group with a similar 6.95×10^{-19} sum of square deviations over a 145 iteration run. Both are summarised in Figure 6.

The resulting best energy group from the PSO was used as the input for the non-stochastic algorithm, which was run over 250 iterations with increasing `nps` and decreasing tension, from 5E5 to 1E7 and 0.2 to 0.05, respectively. The square PW-MG deviation in each bin is summarised in Figure 7.

The sum of square PW-MG deviations was reduced through this optimisation by over 5 orders of magnitude, producing a MG structure which contains a much higher thermal-energy bin density. The total (n,Xt) deviation in the reaction rate has dropped from the Vitamin-J value of 1.2%, to a PSO output deviation of 0.03% and a final optimised deviation which is less than 0.01%. At this point the MG error can no longer be discerned from the statistical uncertainties of the MC simulation.

An optimisation was run with a 69 bin MG[7] with a hand-made non-stochastic seed MG extracted from the 175 output. With considerably fewer groups the MCNP simulation requirements for low-uncertainty calculations were considerably relaxed and the optimisation produced a MG with 0.03% PW-MG reaction rate deviation. The final MG square deviations are shown in Figure 8 against the final 175 MG output. A comparison of the relative number of bins per energy 'decade' is shown in Figure 9. The mean square deviations $\bar{f} = \frac{1}{n}\sum_{i=1}^{n} f_i$ both represent bin-error distributions which have similarly converged, with similar relative errors $var(f_i)/\bar{f} \approx 1$. With more than double the bin density, the 175-group structure possesses less than 1% the $\bar{f}$ of the 69-group. While the total reaction rate deviation does not reflect this difference, due to counteracting under/over-estimations, the substantially lower square deviation of the finer group makes it a more robust MG, less susceptible to increased errors with modifications in geometry, materials and/or flux.

5. Discussion

Collapsed, effective cross sections are required to obtain time-dependent solutions of the Bateman equations, which update nuclide inventories and importantly require regular updates from the neutron spectra to re-calculate the reaction rates. Here, the effect of 1% errors in reaction rates can in general be profound as they add errors into future inventories which result in additional errors in the subsequent transport simulations. This then exacerbates the next cross section errors and the cycle can quickly turn 1% errors into 10% errors (or worse), as demonstrated in the tritium-breeding case of [5].

Note that the distributions in Figure 9 do not agree completely, particularly with the region around the 244 keV resonance of ^{6}Li(n,α)^{3}H. This generally reflects the lack of complete convergence upon our 'ideal' equal deviation-per-bin MG. Due to the fact that the total deviations are too small (with respect to the MC statistical uncertainty) to optimise, we cannot find the ideal and there exists a space of MG energy structures which all possess less PW-MG deviation than can be determined from MCNP calculations with reasonable simulation time. By decreasing the number of bins we can enter a regime where an optimal MG theoretically could be determined.

Working with fewer MG bins generally makes the optimisation much easier to perform. To give an illustration, see Figure 10 with the TRIPOLI-315 MG and the result of 200 iterations of the non-stochastic algorithm which has ordered the deviations into a string but has not decreased the variation in bin error. In this simple formulation, the algorithm is not appropriate for migrating bins, especially where deviations are already so small. The TRIPOLI case provides a more pronounced example of what occurs when attempting to use the string algorithm with Vitamin-J as an initial MG, although in both cases the string algorithm fails to efficiently improve a MG structure with many bins and large regions with substantially different PW-MG errors. This underlines the purpose of the PSO; to find a more suitable seed for the string optimisation which was found to be inefficient in those circumstances. Any alternative process for obtaining such a seed MG would suffice and *in this simple model* such a MG could be obtained by intuitive

[7] Chosen for EASY-II [12] compatability reasons in future work. Note that the WIMS-69 MG does not extend to 14 MeV and cannot be used for D-T fusion analysis.

guesswork. Most cases of interest will include many more nuclides and reactions, making the task of finding such a seed profoundly more challenging.

We have purposefully chosen an example with no narrow resonances and which has relatively little MG-PW error in general. An optimisation with many reactions will certainly possess considerably greater deviations and nearly every application will involve reactions with non-trivial resonances. Self-shielding corrections are implemented ubiquitously and a specific methodology must be chosen, which the optimisation must incorporate. A natural extension of this work would be to use an inventory code such as FISPACT-II [13] to collapse the spectrum with probability table corrections, or an alternative MC transport code which can accept repeated data modification and incorporate MG self-shielding corrections.

6. Summary

An optimisation methodology using PSO with a 'string-tightening' algorithm for minimising deviations between point-wise (PW) and multi-group (MG) convolution has been presented. The algorithms used a combination of NJOY processing and MCNP tallies to calculate reaction rates and took total squared PW-MG deviation over each bin to generate a fitness function. The optimisation can be applied to other systems and reaction sets with the introduction of self-shielding corrections, where necessary.

Optimisation of two MG structures was performed on a simplified concentric sphere model of a magnetic confined fusion reactor. Total tritium production through reactions with ^{6}Li, ^{7}Li and ^{9}Be were used to generate the fitness function. In this simple case, the Vitamin-J structure introduced a 1.2% error *solely* due to the MG convolution. While nuclear data uncertainty may be more significant for some reaction channels, the introduction of unnecessary errors due to poor choices of energy discretisation should be avoided. In time-evolving simulations, these errors will also affect inventories, fluxes, spectra and other quantities which may feedback on the reaction of interest and further magnify the error.

The Vitamin-J group structure is far too coarse in the low-energy range, as it was not designed for representation of neutron spectra for thermal reactions. After optimisation the error was taken down to the statistical uncertainty of the transport simulation. Optimisation for a 69-bin MG resulted in a 0.03% total reaction rate error, while the TRIPOLI 315 MG deviation was at the transport uncertainty without modification. The errors that the Vitamin-J MG introduce can easily be avoided by using an energy structure optimised for an application or a finer MG, such as the TRIPOLI 315 or CCFE 709.

Acknowledgements

Thanks are due to J-Ch. Sublet for guidance and comments, as well as D. Kotlyar for suggestions early in the work. This research has received funding from the RCUK Energy Programme [grant number EP/I501045].

Appendix A. Reference Data

For reference, we include the atomic fractions of the materials which were used in the material specification for the tritium breeding concentric sphere model in Table A.2. The cells are those described in Table 1 and Figure 4. Note that the blanket (cells 3-6) is a homogenised material including the Eurofer steel, beryllium and lithium ceramic, as well as the helium purge and coolant gas. In Table A.3 we list the optimised energy groups with the original Vitamin-J multi-group given for comparison.

Table A.3: Summary of final 175 and 69 bin optimised energy group structures in eV with Vitamin-J included as a reference.

Bin	Vitamin-J	Opt. 175	Opt. 69	Bin	Vitamin-J	Opt. 175
0	1.0000E-05	1.0000E-05	1.0000E-05	88	2.8725E+05	8.5059E+01
1	1.0000E-01	4.2698E-03	1.8432E-02	89	2.8725E+05	8.5059E+01
2	4.1399E-01	9.9754E-03	3.9887E-02	90	2.9452E+05	9.0384E+01
3	5.3158E-01	1.6160E-02	6.2406E-02	91	2.9720E+05	9.6065E+01
4	6.8256E-01	2.3099E-02	8.6862E-02	92	2.9850E+05	1.0188E+02
5	8.7642E-01	3.2352E-02	1.1327E-01	93	3.0197E+05	1.0840E+02
6	1.1254E+00	4.2161E-02	1.4125E-01	94	3.3373E+05	1.1471E+02
7	1.4450E+00	5.2218E-02	1.7345E-01	95	3.6883E+05	1.2247E+02
8	1.8554E+00	6.2806E-02	2.1188E-01	96	3.8774E+05	1.3067E+02
9	2.3824E+00	7.3594E-02	2.5533E-01	97	4.0762E+05	1.3935E+02
10	3.0590E+00	8.4720E-02	3.0502E-01	98	4.5049E+05	1.4883E+02
11	3.9279E+00	9.7018E-02	3.6269E-01	99	4.9787E+05	1.5885E+02
12	5.0435E+00	1.0935E-01	4.3066E-01	100	5.2340E+05	1.6989E+02
13	6.4760E+00	1.2199E-01	5.1152E-01	101	5.5023E+05	1.8333E+02
14	8.3153E+00	1.3577E-01	6.0599E-01	102	5.7844E+05	1.9892E+02
15	1.0677E+01	1.5092E-01	7.1741E-01	103	6.0810E+05	2.1314E+02
16	1.3710E+01	1.6653E-01	8.5057E-01	104	6.3928E+05	2.2724E+02
17	1.7603E+01	1.8328E-01	1.0087E+00	105	6.7206E+05	2.4405E+02
18	2.2603E+01	2.0132E-01	1.2057E+00	106	7.0651E+05	2.6246E+02
19	2.9023E+01	2.2049E-01	1.4445E+00	107	7.4274E+05	2.8202E+02
20	3.7267E+01	2.4096E-01	1.7241E+00	108	7.8082E+05	3.0468E+02
21	4.7851E+01	2.6320E-01	2.0860E+00	109	8.2085E+05	3.2987E+02
22	6.1442E+01	2.8679E-01	2.5212E+00	110	8.6294E+05	3.7235E+02
23	7.8893E+01	3.1196E-01	3.0622E+00	111	9.0718E+05	4.0976E+02
24	1.0130E+02	3.3812E-01	3.7190E+00	112	9.6164E+05	4.4865E+02
25	1.3007E+02	3.6622E-01	4.5394E+00	113	1.0026E+06	4.9102E+02
26	1.6702E+02	3.9592E-01	5.5992E+00	114	1.1080E+06	5.3833E+02
27	2.1445E+02	4.2839E-01	7.0039E+00	115	1.1648E+06	5.9022E+02
28	2.7536E+02	4.6334E-01	8.8197E+00	116	1.2246E+06	6.4878E+02
29	3.5358E+02	5.0184E-01	1.1376E+01	117	1.2873E+06	7.1355E+02
30	4.5400E+02	5.4134E-01	1.4812E+01	118	1.3534E+06	7.8717E+02
31	5.8295E+02	5.8203E-01	1.8194E+01	119	1.4227E+06	8.6802E+02
32	7.4852E+02	6.3113E-01	2.2087E+01	120	1.4957E+06	9.5799E+02
33	9.6112E+02	6.7730E-01	2.9386E+01	121	1.5724E+06	1.0684E+03
34	1.2341E+03	7.3090E-01	4.0376E+01	122	1.6530E+06	1.1983E+03
35	1.5846E+03	7.8609E-01	5.6892E+01	123	1.7377E+06	1.3303E+03
36	2.0347E+03	8.4649E-01	6.7284E+01	124	1.8268E+06	1.4782E+03
37	2.2487E+03	9.1588E-01	7.7404E+01	125	1.9205E+06	1.6415E+03
38	2.4852E+03	9.8811E-01	8.9898E+01	126	2.0190E+06	1.8374E+03
39	2.6126E+03	1.0680E+00	1.0461E+02	127	2.1225E+06	2.1337E+03
40	2.7465E+03	1.1565E+00	1.2208E+02	128	2.2313E+06	2.4503E+03
41	3.0354E+03	1.2519E+00	1.4299E+02	129	2.3069E+06	2.9574E+03
42	3.3546E+03	1.3678E+00	1.6800E+02	130	2.3457E+06	3.5151E+03
43	3.7074E+03	1.4921E+00	1.9770E+02	131	2.3653E+06	4.0631E+03
44	4.3074E+03	1.6125E+00	2.3310E+02	132	2.3852E+06	4.9626E+03
45	5.5308E+03	1.7451E+00	2.7712E+02	133	2.4660E+06	5.8247E+03
46	7.1017E+03	1.8909E+00	3.3474E+02	134	2.5924E+06	7.4219E+03
47	9.1188E+03	2.0539E+00	4.3998E+02	135	2.7253E+06	1.0478E+04
48	1.0595E+04	2.2237E+00	5.5215E+02	136	2.8650E+06	1.3517E+04
49	1.1709E+04	2.4126E+00	6.9877E+02	137	3.0119E+06	1.8046E+04
50	1.5034E+04	2.6141E+00	8.8991E+02	138	3.1664E+06	2.3172E+04

Bin	Vitamin-J	Opt. 175	Opt. 69	Bin	Vitamin-J	Opt. 175
51	1.9305E+04	2.8261E+00	1.1338E+03	139	3.3287E+06	2.6462E+04
52	2.1875E+04	3.0639E+00	1.4851E+03	140	3.6788E+06	2.8876E+04
53	2.3579E+04	3.3170E+00	1.9844E+03	141	4.0657E+06	4.1369E+04
54	2.4176E+04	3.5782E+00	2.9326E+03	142	4.4933E+06	8.6949E+04
55	2.4788E+04	3.8647E+00	4.4149E+03	143	4.7237E+06	1.3271E+05
56	2.6058E+04	4.3572E+00	6.9022E+03	144	4.9659E+06	1.4364E+05
57	2.7000E+04	4.6320E+00	1.2760E+04	145	5.2205E+06	1.6016E+05
58	2.8500E+04	4.9771E+00	2.5729E+04	146	5.4881E+06	1.8268E+05
59	3.1828E+04	5.3663E+00	8.3906E+04	147	5.7695E+06	1.8910E+05
60	3.4307E+04	5.8191E+00	1.9535E+05	148	6.0653E+06	1.9964E+05
61	4.0868E+04	6.5011E+00	2.4511E+05	149	6.3763E+06	2.1186E+05
62	4.6309E+04	6.9427E+00	2.8803E+05	150	6.5924E+06	2.2381E+05
63	5.2475E+04	7.5697E+00	4.5997E+05	151	6.7032E+06	2.5150E+05
64	5.6562E+04	8.1488E+00	1.5131E+06	152	7.0469E+06	2.6505E+05
65	6.7379E+04	9.0600E+00	2.9021E+06	153	7.4082E+06	2.7955E+05
66	7.2000E+04	9.8914E+00	5.1191E+06	154	7.7880E+06	2.9050E+05
67	7.9500E+04	1.1139E+01	8.4061E+06	155	8.1873E+06	3.0122E+05
68	8.2500E+04	1.2527E+01	1.2839E+07	156	8.6071E+06	3.2028E+05
69	8.6517E+04	1.3858E+01	1.9640E+07	157	9.0484E+06	3.3839E+05
70	9.8037E+04	1.5251E+01		158	9.5123E+06	3.8740E+05
71	1.1109E+05	1.6708E+01		159	1.0000E+07	4.6861E+05
72	1.1679E+05	1.8030E+01		160	1.0513E+07	6.0368E+05
73	1.2277E+05	1.8704E+01		161	1.1052E+07	6.9169E+05
74	1.2907E+05	1.9274E+01		162	1.1618E+07	1.4772E+06
75	1.3569E+05	2.1584E+01		163	1.2214E+07	2.3499E+06
76	1.4264E+05	2.3863E+01		164	1.2523E+07	2.7826E+06
77	1.4996E+05	2.7663E+01		165	1.2840E+07	3.2254E+06
78	1.5764E+05	3.1341E+01		166	1.3499E+07	4.1000E+06
79	1.6573E+05	3.5268E+01		167	1.3840E+07	5.2725E+06
80	1.7422E+05	3.9728E+01		168	1.4191E+07	5.9859E+06
81	1.8316E+05	4.6974E+01		169	1.4550E+07	7.8217E+06
82	1.9255E+05	5.2774E+01		170	1.4918E+07	9.9952E+06
83	2.0242E+05	6.0563E+01		171	1.5683E+07	1.1994E+07
84	2.1280E+05	6.4096E+01		172	1.6487E+07	1.3138E+07
85	2.2371E+05	6.7702E+01		173	1.6905E+07	1.3840E+07
86	2.3518E+05	7.1574E+01		174	1.7333E+07	1.4129E+07
87	2.4724E+05	7.5645E+01		175	1.9640E+07	1.9640E+07

References

[1] J. F. Briesmeister, MCNP - A General Monte Carlo N-Particle Transport Code, Version 4C, Los Alamos National Laboratory, USA, LA-UR-05-8225 (December 2000).

[2] L. Morgan, J.-C. Sublet, W. Haeck, J. Pasley, Optimising the energy group structure used for fusion systems, Annals of Nuclear Energy 55 (2013) 108 – 115. doi:http://dx.doi.org/10.1016/j.anucene.2012.11.028.

[3] E. Sartori, Vitamin-j, a 175 group neutron cross section library based on jef-1 for shielding benchmark calculations, Tech. Rep. JEF/DOC-100, NEA Data Bank (October 1985).

[4] P. Vontobel, S. Pelloni, JEF/EFF Based Nuclear Data Libraries, Tech. Rep. EIR-Report 636, Paul Scherrer Institute (December 1987).

[5] A. Aures, L. Packer, S. Zheng, Tritium self-sufficiency of HCPB blanket modules for DEMO considering time-varying neutron flux spectra and material compositions, Fusion Engineering and Design 88 (9-10) (2013) 2436–2439. doi:10.1016/j.fusengdes.2013.05.042.

[6] G. Beni, J. Wang, Swarm intelligence in cellular robotic systems, Proceedings of NATO Advanced Workshop on Robots and Biological Systems.

[7] J. Kennedy, R. Eberhart, Particle swarm optimization, Proceedings of IEEE International Conference on Neural Networks 4 (1995) 1942 – 1948.

[8] R. E. MacFarlane, A. Kahler, The NJOY Nuclear Data Processing System, Version 2012, Los Alamos National Laboratory, LA-UR-12-27079 (December 2012).

[9] I. Bondarenko, Group Constants for Nuclear Reactor Calculations, Consultants Bureau, 1964.

[10] R. E. MacFarlane, TRANSX 2: A Code for Interfacing MATXS Cross-Section Libraries to Nuclear Transport Codes, Los Alamos National Laboratory, LA-12312-MS (July 1992).

[11] L. Giancarli, M. Abdou, D. Campbell, V. Chuyanov, M. Ahn, M. Enoeda, C. Pan, Y. Poitevin, E. Rajendra Kumar, I. Ricapito, Y. Strebkov, S. Suzuki, P. Wong, M. Zmitko, Overview of the ITER TBM Program, Fusion Engineering and Design 87 (5-6) (2012) 395–402. doi:10.1016/j.fusengdes.2011.11.005.

[12] J.-C. Sublet, J. Eastwood, G. Morgan, A. Koning, D. Rochman, EASY-II: a system for modelling of n, d, p, γ and α activation and transmutation processes, Joint International Conference on Supercomputing in Nuclear Applications and Monte Carlodoi:http://dx.doi.org/10.1051/snamc/201402103.

[13] J.-Ch. Sublet, J. W. Eastwood, J. G. Morgan, The FISPACT-II User Manual, Tech. Rep. CCFE-R(11) 11 Issue 6, CCFE (2014).

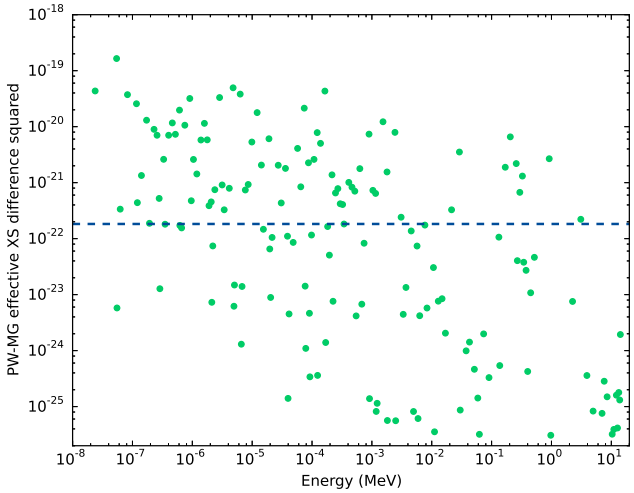

Figure 1: Particle swarm output multi-group square deviations example against the deviation per bin for the 'ideal' 175 group solution in blue.

Table 1: Cellular break-down of tritium breeding reactor model with homogenised blanket layers by % volume.

Cell(s)	Outer Radii (cm)	Material Composition
1	1000	Void
2	1005	First wall
3,4,5,6	1020,1035,1050,1065	55% Be, 10% Eurofer, 20% He, 15% $LiSO_4$
7	1105	80% Eurofer, 20% He
8	1145	80% Inconel-718, 20% He
9	1365	70% NbSn Coil, 20% He 10% Inconel-718

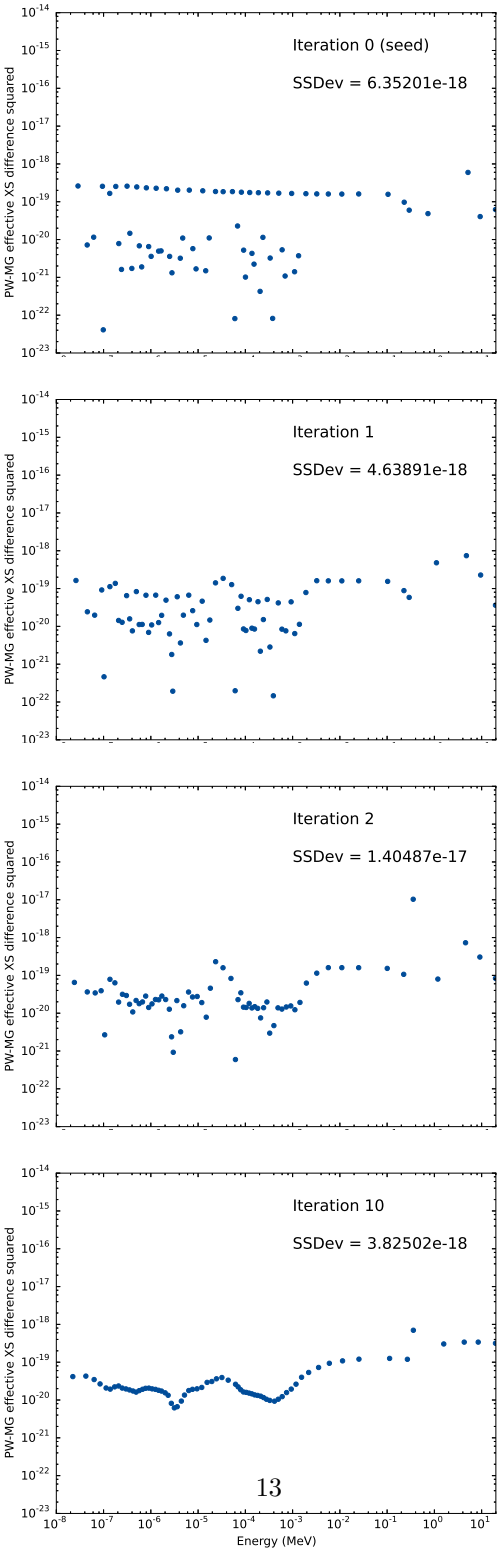

Figure 2: Example of evolution over non-stochastic algorithm with 69-group energy structure. Iterations 0, 1, 2 and 10 are shown.

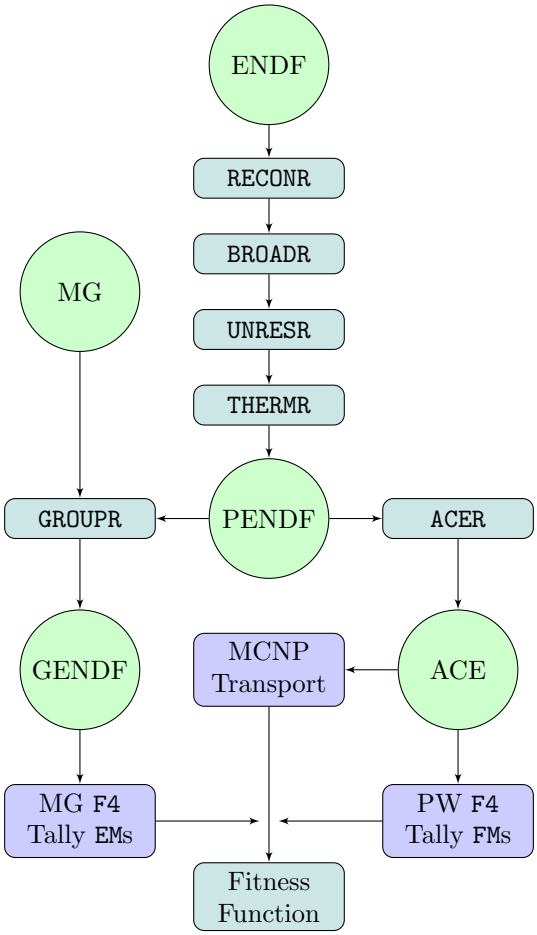

Figure 3: Flowchart of NJOY module execution and use of outputs.

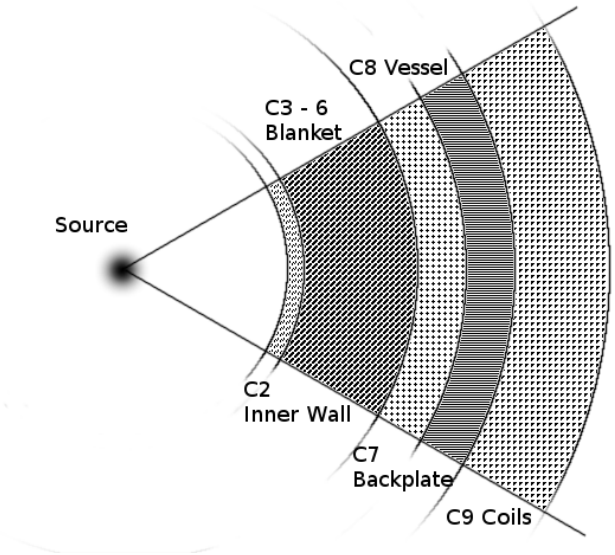

Figure 4: Geometric cross-section of the tritium breeding sphere model with homogenised blankets (not to scale).

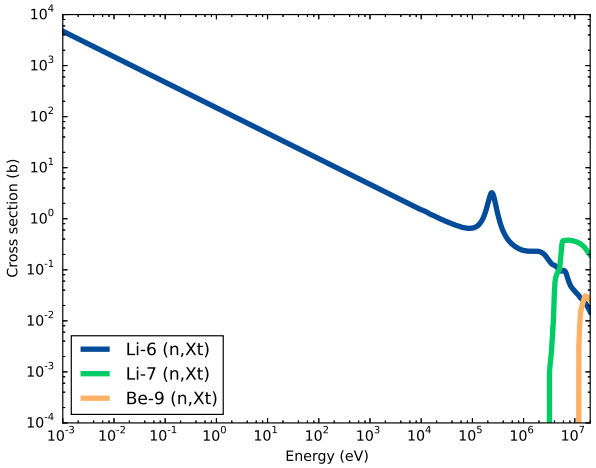

Figure 5: Point-wise cross-sections for total tritium production reactions within the breeding blanket.

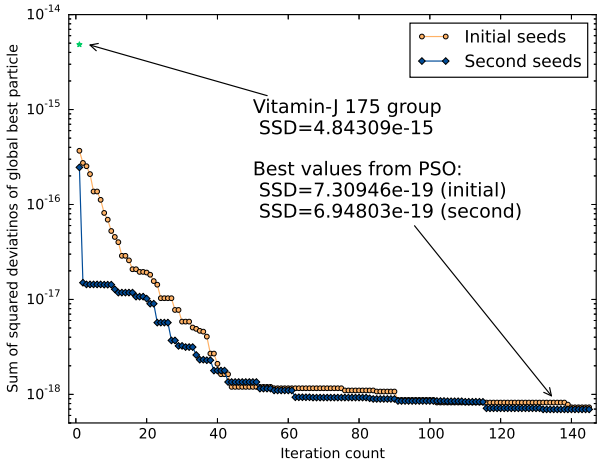

Figure 6: Global best sum of squared PW/MG deviations over PSO runs.

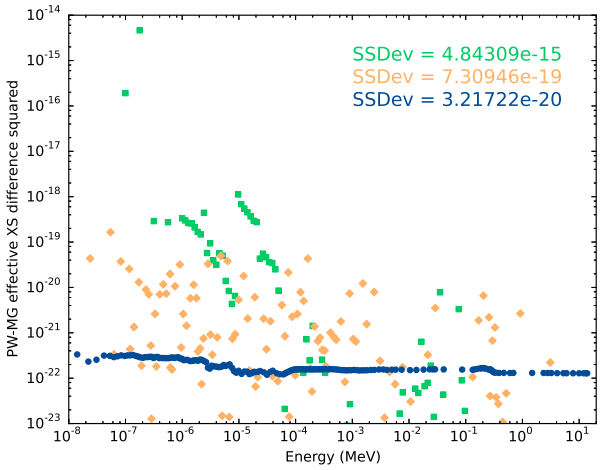

Figure 7: Square PW/MG deviations over the 175 group PSO and non-stochastic optimisation. The multi-groups shown are, from worst to best, the Vitamin-J structure, the PSO output and the final energy group.

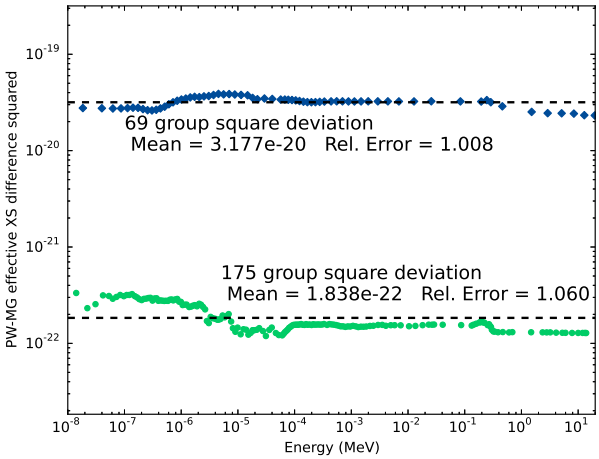

Figure 8: Square deviations for each bin in final energy groups against corresponding mean square deviations.

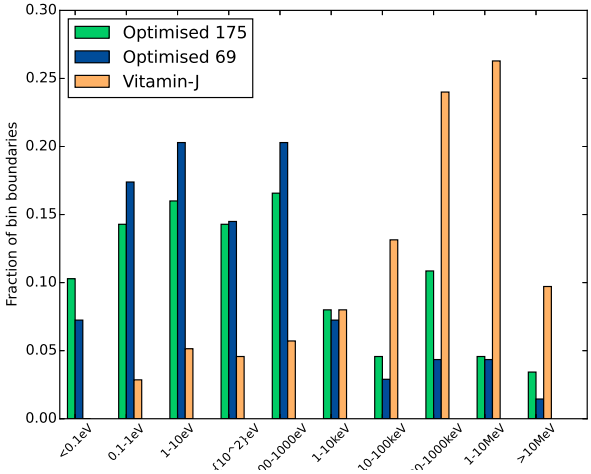

Figure 9: Distribution of energy bins by decade for the 69 optimised structure compared with the optimised 175 and Vitamin-J multi-groups.

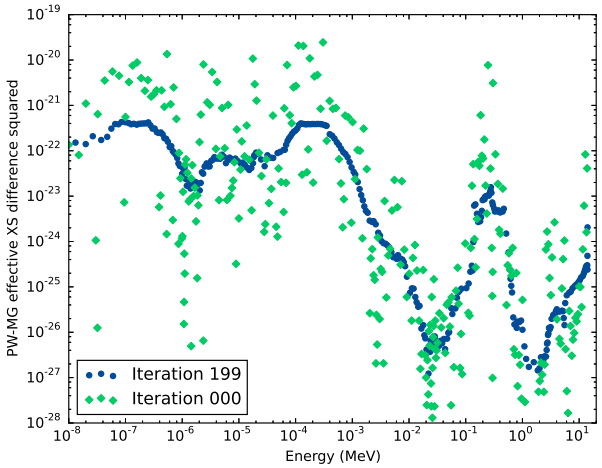

Figure 10: Evolution of TRIPOLI 315 multi-group square deviations over 200 iterations of the non-stochastic optimisation.

Table A.2: Simplified DEMO-like model atom fractions by cell and densities in g/cm^3.

	Cell 2	Cells 3-6	Cell 7	Cell 8	Cell 9
Density	7.528	2.131	6.296	6.577	6.313
^{3}He	2.10019E-11	7.48667E-11	9.97068E-11	1.00395E-10	1.02771E-10
^{4}He	1.50014E-05	5.34762E-05	7.12191E-05	7.17109E-05	7.34075E-05
^{6}Li		5.50544E-03			
^{7}Li		6.79004E-02			
^{9}Be		7.36907E-01			
^{12}C	5.20676E-03	5.15578E-04	5.49313E-03		
^{13}C	5.84437E-05	5.78715E-06	6.16582E-05		
^{14}N	1.68695E-03	1.67043E-04	1.77973E-03		
^{15}N	6.19691E-06	6.13623E-07	6.53774E-06		
^{16}O	3.29352E-04	7.70772E-02	3.47466E-04		
^{17}O	1.25455E-07	2.93598E-05	1.32355E-07		
^{50}Cr	4.16488E-03	4.09970E-04	4.36796E-03	9.18855E-03	7.43317E-03
^{52}Cr	8.11668E-02	7.98965E-03	8.51244E-02	1.79070E-01	1.44860E-01
^{53}Cr	9.20149E-03	9.05748E-04	9.65014E-03	2.03003E-02	1.64221E-02
^{54}Cr	2.32459E-03	2.28821E-04	2.43793E-03	5.12850E-03	4.14874E-03
^{55}Mn	5.75567E-03	5.69931E-04	6.07223E-03		
^{54}Fe	4.82666E-02	4.77940E-03	5.09213E-02	1.09324E-02	3.41673E-02
^{56}Fe	7.63944E-01	7.56464E-02	8.05961E-01	1.73034E-01	5.40786E-01
^{57}Fe	1.74758E-02	1.73047E-03	1.84370E-02	3.95829E-03	1.23709E-02
^{58}Fe	2.49655E-03	2.47210E-04	2.63386E-03	5.65470E-04	1.76727E-03
^{58}Ni				3.73181E-01	1.17162E-01
^{60}Ni				1.43573E-01	4.50756E-02
^{61}Ni				6.02789E-03	1.89249E-03
^{62}Ni				1.97276E-02	6.19359E-03
^{64}Ni				5.47990E-03	1.72044E-03
^{63}Cu	3.56780E-02				2.00289E-02
^{65}Cu	1.58798E-02				8.91461E-03
^{90}Zr	2.80384E-05				
^{91}Zr	6.09768E-06				
^{92}Zr	9.30985E-06				
^{94}Zr	9.47318E-06				
^{96}Zr	1.52442E-06				
^{93}Nb				3.14727E-02	2.71051E-02
^{92}Mo				2.70666E-03	3.46338E-04
^{94}Mo				1.70081E-03	2.17631E-04
^{95}Mo				2.90784E-03	3.72079E-04
^{96}Mo				3.05414E-03	3.90800E-04
^{97}Mo				1.75567E-03	2.24651E-04
^{98}Mo				4.40747E-03	5.63969E-04
^{100}Mo				1.75567E-03	2.24651E-04
^{112}Sn					7.61289E-05
^{114}Sn					5.05014E-05
^{115}Sn					2.86426E-05
^{116}Sn					1.10048E-03
^{117}Sn					5.84158E-04
^{118}Sn					1.83840E-03
^{119}Sn					6.48227E-04
^{120}Sn					2.44216E-03
^{122}Sn					3.43711E-04
^{124}Sn					4.25116E-04
^{181}W	2.62124E-04	2.59557E-05	2.76541E-04		
^{182}W	9.04794E-04	8.95935E-05	9.54558E-04		
^{183}W	4.92522E-04	4.87700E-05	5.19611E-04		
^{184}W	1.05737E-03	1.04702E-04	1.11553E-03		
^{186}W	9.85044E-04	9.75399E-05	1.03922E-03		